Recent Advances in Bismuth Oxychalcogenides Nanosheets for Sensing Applications

Journal:	*Nanoscale*
Manuscript ID	NR-MRV-02-2024-000821.R1
Article Type:	Minireview
Date Submitted by the Author:	22-Apr-2024
Complete List of Authors:	Shringi, Amit Kumar; North Carolina Central University Kumar, Rajeev; North Carolina Central University Yan, Fei; North Carolina Central University, Chemistry & Biochemistry

Recent Advances in Bismuth Oxychalcogenides Nanosheets for Sensing Applications

Amit Kumar Shringi, Rajeev Kumar, Fei Yan

Department of Chemistry and Biochemistry, North Carolina Central University, Durham-27707, North Carolina, United States

Abstract

This review offers insights into the fundamental properties of bismuth oxychalcogenides Bi_2O_2X (X = S, Se, Te) (BOX), concentrating on recent advancements primarily from studies published over the past five years. It examines the physical characteristics of these materials, synthesis methods, and their potential as critical components for gas sensing, biosensing, and optical sensing applications. Moreover, it underscores the implications of these advancements for the development of military, environmental, and health monitoring devices.

1. Introduction

The semiconductor industry has been ruled by silicon since 1950 due to its excellent electronic properties, stability, and abundance on Earth's crust.[1] Over the years, silicon technology evolved very fast and matured with the extensive efforts of researchers and the wide acceptance of electronic applications. Silicon-based technologies downscaled to 5 nm by 2020 and further downscaling efforts are in progress.[2] But silicon as a 3D semiconductor seems to be hitting the downscaling limit and fabrication challenges. The reduced carrier mobility and power dissipation are the major challenges associated with silicon technology at lower feature sizes. The use of lower-dimensional semiconductors can be a potential solution for future electronics. Low-dimensional materials offer high carrier mobility, minimal scattering and can be downscaled up to 1 nm.[3] These low-dimensional semiconductors show multifunctional properties and can be used for other semiconductor device applications such as photodetection, sensing, energy storage and memories.[4–7]

In 2004, the discovery of graphene and its surprisingly excellent properties gained huge attention from researchers and industry towards two-dimensional (2D) materials.[8] 2D materials have an atomic-level arrangement and strong interatomic bonds along the two dimensions. The motion of electrons and phonons is confined in the 2D plane with the atomically thin third dimension. The atomically thin 2D materials show fascinating optical, electronic and mechanical features in comparison to their 3D allotrope.[9,10] Layer-modulated band gap transition, and improved atomic contribution for the exposed surface in 2D materials, make them the material of choice for optoelectronic and sensing applications. As a contribution of years of research, a variety of 2D materials have been explored with diverse electronic properties ranging from conductors to insulators. The family of 2D materials evolved over the years and along with graphene, it involves 2D transition metal dichalcogenides (TMDs), MXenes, graphitic carbon nitride (g-C_3N_4), black phosphorus (BP), hexagonal boron nitride (hBN), layered perovskites, and metal phosphorus trichalcogenides.[11–17] These 2D materials have been explored and studied to investigate their material properties and potential for sensing, optoelectronic, storage, catalysis, memory and dielectric applications. Except for the excellent properties as described above, studies also show the limitations associated with these 2D materials. 2D TMDs offer layer-modulated bandgap but these materials suffer from low room temperature carrier mobility, thus limiting their use.[18–20] On the other hand, mobility for graphene (>10000 $cm^2 V^{-1} s^{-1}$) is very high, but a small on/off ratio due to zero bandgap is a limiting factor for electronic uses.[21,22] BP has excellent mobility and wide tunability of band gap but it has issues of instability and processing limiting its practical implementation as a semiconductor.[23,24] Most of these 2D materials are van der Waals (vdW) materials and their interlayer gap leads to high air sensitivity, instability and poor performance. The limitations associated with 2D materials limit their use for sensing applications Hence, it is a requirement of time to explore, design and investigate new 2D materials with tunable electronic properties, high carrier mobility, processibility and environmental stability for the realization of next-generation semiconductor devices.

Recently, novel 2D bismuth oxychalcogenides (BOXs) caught significant attention due to excellent physical and chemical properties such as high-carrier mobility, environmental stability, band gap tunability and quick response to external signals.[25,26] BOXs comprise alternate stacks of $[Bi_2O_2]^{2+}$ and $[X]^{2-}$(X= S, Se, Te) that are adhered through weak electrostatic force. Due to excellent absorption of light and bandgap ranging from 0.11 to 1.6 eV, BOXs have been extensively explored for photodetection applications.[27] BOXs offer high mobility in ambient conditions with a decent band gap range, that makes them the material of choice for the fabrication of resistive sensors for room temperature detection having a high signal-to-noise ratio.[28,29] Further, the recent progress in wafer-scale growth of crystalline Bi_2O_2Se shows the potential of integration of these materials with Si technology in the near future.[30]

The ultrahigh carrier mobility, bandgap range, and excellent stability towards environmental conditions make BOXs a material of choice over other semiconductors for sensing and optoelectronic applications. In recent years many synthesis approaches such as sol-gel, hydrothermal, chemical vapor deposition (CVD), molecular beam epitaxy (MBE), etc. have been explored for the realization of BOXs for different applications. The theoretical and experimental observations from recent reports show the potential of these materials as sensors for gas, bio, electrochemical and optical sensing.

In this review article, we will discuss the recent progress of BOXs referring to synthesis, growth and sensing applications. The different synthesis approaches including CVD, pulsed laser deposition (PLD) and exfoliation will be discussed. Crystal structure, electronic band structure along with the other material and electronic properties like carrier mobility, optical properties and ferroelectricity are briefly discussed for a general understanding of material behaviour towards different applications. In the next section, we discussed the most recent reports for BOXs-based sensing applications. We broadly classified the sensing application into three categories namely gas sensing, bio sensing and optical sensing for the ease of audience.

2. Atomic Structure and Material Properties

2.1 Atomic Structure

BOXs are non-vdW layered materials where each unit consists of two [Bi_2O_2] layers between three atomic layers of chalcogen elements. The monolayer thick BOXs has one [Bi_2O_2] cation layer between two chalcogen anion layers where 50% of chalcogen atoms of the chalcogen layer are shared with another monolayer and have a covalent bond with weak electrostatic interaction between layers. The atomic representation of BOXs is given in Fig. 1a. According to the atomic arrangement, Bi_2O_2S crystals have orthorhombic structure and Pnnm space group (a = 3.874 Å, b = 3.84 Å and c = 11.92 Å) whereas the Bi_2O_2Se and Bi_2O_2Te have tetragonal crystal structure with I3/mmm space group. The lattice parameter a = b = 3.88 Å, c = 12.16 Å and Z = 2 for Bi_2O_2Se and a = b = 3.98 Å, c = 12.70 Å for Bi_2O_2Te. Bulk BOXs crystals can be cleaved or exfoliated along the c-axis because of their non-neutral layered structure and appear in broken zipper structure where half of the chalcogen atoms are shared by each part of the BiO^+ layer as shown in Fig. 1b.[31]

2.2 Electronic Band Structure and Optical Properties:

Wu et al. reported the theoretical calculations to predict the electronic band structure of BOXs. The calculated values as shown in Fig 1c-e were 1.25 eV for Bi_2O_2S, 0.89 eV for Bi_2O_2Se and 0.16 eV for Bi_2O_2Te.[32] All three compounds show the indirect band gap. The experimental band gap calculated using the Tauc plot shows a band gap of 1.3 eV to 1.5 eV referred to in different reports for Bi_2O_2S.[33,34] Considering the indirect nature of the band gap, the experimental band gap reported is 1.38 eV to 1.67 eV for Bi_2O_2Se.[35,36] The optical band gap of Bi_2O_2Te is still unknown so far due to the synthesis complexity for producing bulk and large-area samples.

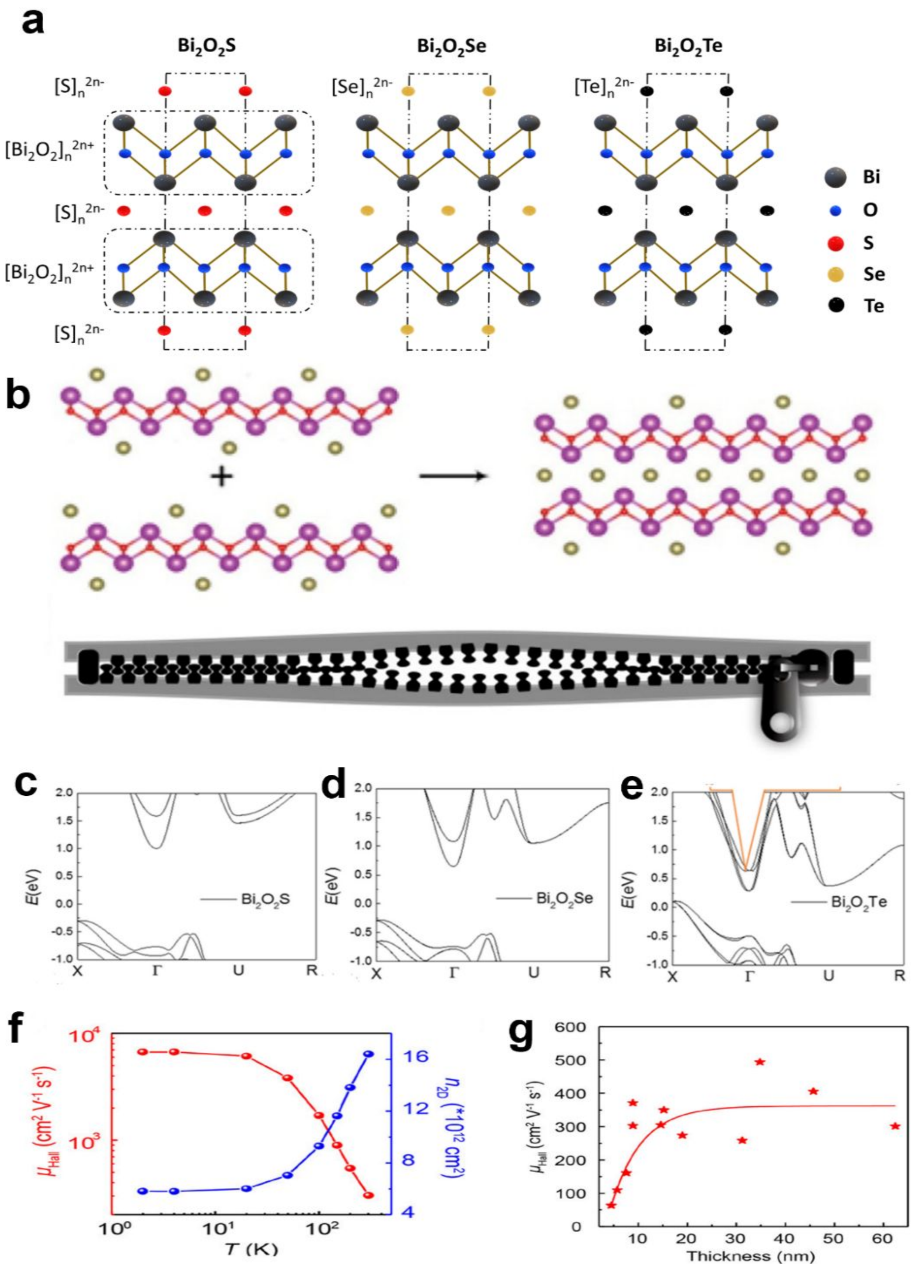

Fig. 1 (a) Crystal structures of Bi_2O_2S, Bi_2O_2Se and Bi_2O_2Te. (b) Scheme of a bilayer Bi_2O_2Se formed by two monolayers and a zipper model. Reproduced with permission.[31] Copyright 2019, American Chemical Society. Electronic band structure (c) Bi_2O_2S, (d) Bi_2O_2Se and (e) Bi_2O_2Te. Reproduced with permission.[32] Copyright 2019, American Chemical Society. (f-g) Temperature and thickness dependent carrier mobility of Bi_2O_2Te. Reproduced with permission.[38] Copyright 2022, American Chemical Society.

2.3 Carrier Concentration and Mobility

The theoretical report shows ultrahigh electron mobility can be upto 26699 $cm^2 V^{-1} s^{-1}$ at 330 K for Bi_2O_2S monolayer but still hasn't been explored experimentally.[39] Bi_2O_2Se shows ultrahigh electron mobility of 20000 $cm^2 V^{-1} s^{-1}$ and carrier concentration of 5×10^{18} cm^{-3} at 2 K. The room temperature mobility of 313 $cm^2 V^{-1} s^{-1}$ and carrier density of 11×10^{18} cm^{-3} was reported.[40] Temperature and thickness-dependent mobility for Bi_2O_2Te is represented in Fig 1f. The carrier mobility of 303 $cm^2 V^{-1} s^{-1}$ and the carrier density of 1×10^{13} cm^{-3} at RT for 8.9 nm thick Bi_2O_2Te nanosheets.[38] The experimental results show the variation in mobility and carrier density and it strongly depends on the different parameters like thickness, defect density and temperature. It is still desirable to develop advanced growth and modification strategies to achieve ultrahigh mobility and high carrier density at RT.

The high mobility in BOXs compared to other semiconductors led to the donor states lying above the lowest conduction band. Fu et al. observed the spontaneous ionization of electrons from donor sites for Bi_2O_2Se even without any thermal activation resulting in reduced resistance upon reduction in temperature.[41] The spatial separation of the conduction channel from the ionized donor defects further suppresses the donor sites led scattering, resulting in further increased electron mobility. They call this phenomenon spontaneous self-modulation doping. Similarly, Tong et al. observed the 10x transport lifetime due to suppressed backward scattering of electrons in Bi_2O_2Se resulting in ultrahigh electron mobility.[42]

2.4 Other Properties

There are several other properties except for structural, electronic and charge mobility, that have great significance for the application of a semiconductor material. Ferroelectricity is an important property for a semiconductor material enabling its use for sensing, storage and energy applications. The existence of ferroelectricity has been predicted theoretically for BOXs.[32] It has been experimentally demonstrated for 2D Bi_2O_2Se and Bi_2O_2Te nanosheets, where they have spontaneous polarization and show switching under an external electric field.[43,44]

The environmental stability of a sensing material is an important factor to be taken care of and it has a direct relation to its real-time application. As discussed in the introduction, 2D semiconductors like BP have excellent carrier mobility but environmental instability is a limiting factor for its use for environmental monitoring applications. On the other hand, 2D BOXs have been reported for ultrahigh carrier mobility with excellent stability in ambient conditions.[45,46] Stable electronic properties upon exposure to ambient conditions with high mobility make them promising materials for environmental monitoring applications.

The biocompatibility of nanomaterials is an important aspect to be considered before using them for health monitoring, water treatment and therapy applications. Bi_2O_2Se nanosheets have been reported as biosafe material for water treatment[47] and cancer therapy[48] and hence they can be used for biomedical and biosensing applications.

As these materials are new and require a lot of effort to validate and establish the reason behind these properties. Due to limited experimental evidence, BOXs have not been studied for energy harvesting applications. BOXs show excellent atmospheric stability compared to other 2D materials and pertain to excellent flexibility without affecting the electronic properties.

3. Synthesis of 2D BOXs

The performance of 2D material-based electronic devices highly depends on the quality of synthesized material as it alters the chemical and physical properties of these materials. Hence, a lot of research efforts have been made with time to develop the protocols for large-scale and low-cost synthesis or growth of high-quality 2D materials. To date, various approaches have been reported for the synthesis and growth of 2D BOXs. The synthesis approaches for 2D BOXs are broadly classified into two categories: bottom-up, and top-down approach. Bottom-up approaches of synthesis, where the synthesis involves the chemical precursors of the constituent elements and other reducing and capping agents. Using this approach, the synthesis of powdered material and direct film growth can be achieved. The bottom-up approach involves hydrothermal, solution-assisted methods, CVD, PLD, and molecular beam epitaxy (MBE). The use of different synthesis approaches depends on the application and it significantly alters the cost of the process. Secondly, the top-down approach involved the exfoliation of nanosheets from the bulk material or single crystal of the material. Mechanical exfoliation, liquid exfoliation and ion intercalation are typical examples of top-down methods. The force induced during different methods helps to overcome the weak interlayer bonds to get mono or few-layer nanosheets from bulk material. In the coming subsections, we will discuss the various synthesis methods for the synthesis or growth of different BOXs species.

3.1 Bottom-up Processes

3.1.1 Hydrothermal Method

Hydrothermal reaction is a widely used synthesis method to obtain nanostructured materials. It offers a simple, low-cost, high yield and reproducible synthesis. It uses a special closed reaction vessel to execute the synthesis reaction, where the reactions take place at elevated temperatures (80-240 °C) and very high pressure. The temperature and high-pressure environment in the vessel enable the formation and recrystallization of the desired compound. The hydrothermal method offers both powder synthesis and direct growth on a substrate. Zhang et. al. reported the composite molten salt approach for the synthesis of Bi_2O_2Se nanosheets and analyzed the thermoelectric properties. They used KNO_3 and $LiNO_3$ (57.6:42.4) as composite molten salts.[49] Initially, 9 g of salt composite, 1 mmol $Bi(NO_3)_3$•$5H_2O$ and 0.5 mmol Se powder were placed and shaken in 25 ml Teflon vessel for complete mixing of reactants. Further, 2 ml of N_2H_4•H_2O and 5 mL DI water were added and sealed Teflon vessel with a stainless autoclave was put into a preheated oven at 200° C for 24 h. After 24 h, the autoclave was naturally cooled and the obtained solid product was washed with DI water and ethanol using centrifugation. The obtained powder shows sheets-like morphologies with an approximate thickness of 120 nm. In 2020, Li et al. reported the mild hydrothermal route as shown in Fig. 2(a) for synthesizing Bi_2O_2S and Bi_2O_2Se nanosheets.[37] He used the ammonium bismuth citrate, thiourea and sodium selenite as starting precursors for the reaction and KOH as a mineralizer. The stoichiometric ratio of Bi, Se/S sources were dissolved in DI water and KOH was added for an alkali environment. The solution was transferred and sealed in a hydrothermal reactor and the obtained powder was washed several times with DI water and ethanol. The obtained nanosheets have lateral sizes over 2 μm and a thickness ~5 nm (Fig. 2(b-e)).

Except for the powder synthesis, direct growth of Bi_2O_2S nanoflowers and sheets on FTO has been reported by Rong et al. in the year 2022.[50] Equimolar (1 mmol) amounts of thiourea and $Bi(NO_3)_3$•$5H_2O$ were dissolved in a mixture of ethylene glycol and DI water (1:1) for 5 minutes followed by the addition of 5 mmol KOH with continuous stirring until a clear solution was obtained. The solution was transferred to a 50 ml Teflon vessel and a clean FTO substrate was placed at an angle of 30°. The sealed reactor was put in the oven for 3 h at 120° C. Finally, the cooled substrate was taken out and washed with DI water and ethanol followed by natural drying.

The gradual assembly of nanosheets stacking with increased reaction time forming flower-like continuous morphologies. Recently, Zhang et al. reported the growth of Bi_2O_2S nanosheets on FTO with a similar modified growth protocol.[51]

3.1.2 Solution-Assisted Synthesis

The use of a reaction vessel and heating arrangement in the hydrothermal approach makes the process a little complex and costly. The solution-assisted synthesis method offers great simplicity of the process, a low-cost and high-yield solution for the synthesis of various BOXs. The schematic representation and process flow for the synthesis of Bi_2O_2S nanosheets is shown in Fig. 2(f-g).[52] Among all the synthesis methods, the solution-assisted method gained more attention and was explored several times owing to the simple synthesis approach in a beaker over a hot plate (stirrer). Most of the solution-assisted synthesis reports addressed the room temperature synthesis protocol for BOXs, where they used $Bi(NO_3)_3{\cdot}5H_2O$ as a source of Bismuth. On the other hand, different precursors have been reported as sources of chalcogens.

Chitara et al. reported the morphological dependence on the use of a reducing agent for the synthesis of Bi_2O_2S nanostructures.[53] The use of hydrazine hydrate with thiourea led to the formation of nanosheets, whereas in the absence of hydrazine hydrate, thicker nanoplatelets formed. They also observed the change in photoconductivity with the morphology change. Similarly, the use of Se powder with hydrazine hydrate instead of thiourea will lead to the formation of Bi_2O_2Se nanosheets. Recently, Kumar et al. reported the microwave-assisted solution synthesis protocol for Bi_2O_2Te nanosheets.[54] They observed the effect of microwave power on the crystallinity and other properties of the material.

3.1.3 Chemical Vapor Deposition:

CVD is the most popular growth technique for the growth of various 2D materials and it gained significant attention for the growth of high-quality BOXs. It offers a controlled thickness and atomically flat surface. A variety of precursors have been studied and optimized for the growth of BOXs. The carrier gas is used to transfer the vapor of chemical precursor at an elevated temperature to grow the material on the desired solid substrate. The chemical reaction occurs in the gas phase before or during the growth on the substrate. Numerous efforts have been made to develop growth strategies for the growth of BOXs.

For the growth of BOXs, Bi_2O_3 and Bi_2X_3 (X=S, Se, Te) are the commonly used precursors. Further, instead of bismuth chalcogenides elemental precursors can also be used for the growth of BOXs. Ai et al. reported the low-pressure CVD growth of single crystalline 2D Bi_2O_2Te nanoplates.[38] 0.5 g Te and 1 g Bi_2O_3 powder were evaporated in the presence of carrier gas (Ar/Ar: O_2) to Bi_2O_2 and Te layers to form Bi_2O_2Te as shown in Fig. 2(h-i). The ratio of carrier gas (Ar to O_2) and the temperature shows a significant effect on the phase evolution from Bi_2Te_3 to Bi_2O_2Te. Similarly for the CVD growth of Bi_2O_2Se, Chen et al. used Bi_2O_3 and Bi_2Se_3 powder and N_2 as carrier gas.[55] The temperature of Bi_2Se_3 in the first zone was kept at 560° C and Bi_2O_3 in the second zone was kept at 660° C. The effect of narrowing of the growth tube and second zone temperature has a significant effect on the growth thickness. Khan et al. reported the vapor-solid deposition of Bi_2O_2Se using CVD.[56] It uses bulk Bi_2O_2Se powder prepared by hydrothermal method. This approach reduces the requirement of multizone CVD and a controlled system. Single zone CVD is sufficient for the growth of 2D Bi_2O_2Se using this approach.

3.1.4 Pulsed Laser Deposition

The PVD technique is used to deposit a thin film with the same stoichiometry as of source (target). It uses a focused intense laser on the target to vaporize the material in a high vacuum atmosphere inside the chamber. The evaporated material inside the chamber gets deposited onto the substrate. It is a popular and very well-explored technique for the deposition of metal oxides and other materials. In recent years, few reports published on the deposition of Bi_2O_2Se thin films by the PLD method.[57,58] Song et al. reported the deposition of a single crystalline Bi_2O_2Se thin film on a single crystal $SrTiO_3$ substrate.[58] This technique offers a lower growth temperature for BOXs with good control of thickness and stoichiometry.

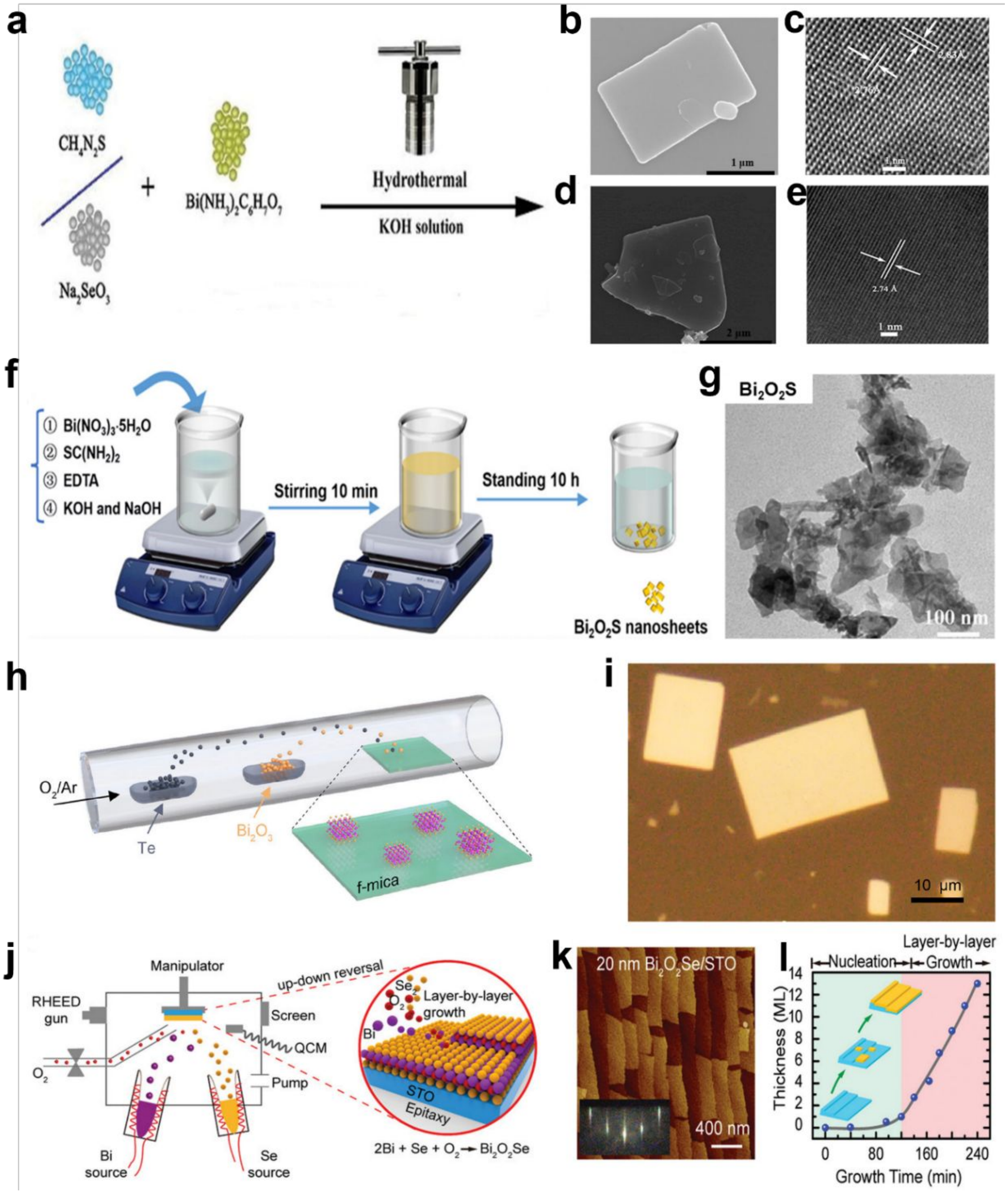

Fig. 2 Synthesis and growth process for 2D BOXs (a) Schematic representation of hydrothermal approach for 2D Bi_2O_2S and Bi_2O_2Se synthesis (b-c) SEM and TEM for Bi_2O_2S (d-e) SEM and TEM for Bi_2O_2Se nanosheets. Reproduced with permission.[37] Copyright 2020, willey-VCH. (f-g) Solution-assisted synthesis of Bi_2O_2S and SEM images of nanosheets. Reproduced with permission.[52] Copyright 2023, American Chemical Society. (h-i) Illustration of CVD growth of 2D Bi_2O_2Te and optical image of Bi_2O_2Te on Mica. Reproduced with permission.[38] Copyright 2022, American Chemical Society. (j-l) Molecular beam epitaxy. Reproduced with permission.[29] Copyright 2020, willey-VCH.

3.1.5 Molecular Beam Epitaxy:

MBE is an advanced growth technique for epitaxial growth of semiconductor thin films with atomic thickness. It offers excellent control of thickness, crystal defects and stoichiometry. MBE growth has been studied and reported many times for the growth of bismuth chalcogenide and it has immense opportunity to explore the potential of MBE growth of BOXs. In 2019, Liang et al. reported the atomically thin Bi_2O_2Se thin film using MBE (Fig. 2(j-l).[29] The growth of Bi_2O_2Se thin film depends on growth parameters like temperature, Bi/Se flux ratio and oxygen ratio. The growth parameters were optimized to $T_s = 290°$ C and oxygen pressure of 1×10^{-4} mbar. The flux ratio needs to be maintained low to avoid the formation of any oxide phase during growth.

Growth temperature and oxygen pressure are important parameters for obtaining controlled thickness over the surface for the growth of phase-pure BOXs layers. For the uniform growth of BOXs, the growth temperature should lie between the evaporation temperature of Bi and X atoms. The evaporation temperature for Te is relatively higher than S and Se, and may need a higher growth temperature for the deposition of Bi_2O_2Te. The growth process for Bi_2O_2Te and Bi_2O_2S has not been explored so far but it has a lot of opportunities to grow these materials using MBE technique.

3.1.6 Other methods

BOXs growth has been reported by several other methods including sputtering, MOCVD and LPCVD.[59,60] Sputtering involves the growth of bismuth chalcogenide followed by oxidation in the air to form BOXs.

3.2 Top-Down Process

The ultrasonic exfoliation of crystal or bulk material into 2D nanosheets or unit geometry using bath or tip sonication is an example of top top-down approach. The exfoliation can be used to reduce the particle size upto quantum dots (QD) dimension.[61] Pan et al. reported the large area nanosheet exfoliation protocol of 20-30 layers thick using bulk Bi_2O_2Se.[62] Hui et al. reported the exfoliated Bi_2O_2Te nanosheets.[63] Tip sonication has been reported to achieve the Bi_2O_2Se QDs and has extensive use for surface functionalization for sensing applications.[64]

Ion intercalation is also a top-down process that involves the intercalating agent intercalating along the thickness of 2D materials and causing the expansion or weakening of the interlayer interaction. With shear force, the interlayer spacing increased further and led to the formation of thin layers from bulk samples. Lithium intercalation has been reported to exfoliate 2D Bi_2O_2Se nanosheets using shear force in a liquid medium.[65] However mechanical exfoliation (tape exfoliation) has not been reported so far for BOXs. The high inter-layer binding energy for BOXs compared to other vdW materials limits the use of scotch tape for exfoliation and needs advanced exfoliation methods for mechanical exfoliation.

In contrast, a variety of synthesis and growth approaches have been explored for the BOXs and each of the methods has its merits and demerits. As discussed in this section, the preparation method significantly alters the morphological and structural properties, such as crystallite size, nanostructure and dimension. One can adopt suitable methods as per the requirement of the application. The top-down approaches including liquid exfoliation, mechanical exfoliation and intercalation, are suitable for achieving BOXs nanosheets with thickness ranging from monolayer to hundreds of layers for bulk material. Mechanical exfoliation offers ultrathin nanosheets of millimeter dimension depending on an individual's expertise. Top-down approaches are low-cost methods and can process large amounts of samples with the same crystallographic phase as bulk materials. However, these methods suffer from the issue of precise control of thickness and reproducibility.

The solution-assisted and hydrothermal approaches are the high-yield and low-cost methods for the synthesis and growth of BOXs nanosheets. The modification in the synthesis method can significantly alter the size and shape of the nanosheets. However, the solution-assisted synthesis approach suffers from the issue of the intermediate phase formation during synthesis. CVD is the widely explored deposition technique used for the growth of BOXs with excellent control of surface morphology and thickness. It is a low-cost deposition method for large-scale high-quality thin films. MBE and PLD growth techniques have been studied for the epitaxial growth of BOXs thin films and are capable of growing high-quality wafer-scale thin films with price control for use in industrial applications. Sophisticated instrumentation, high running cost and requirement of skilled professionals are the limiting factors for these techniques.

4. Sensing Applications

Sensing can be applied for the detection of different analytes, molecules and radiation in different sensing media.[66–68] BOXs have gained huge attention for sensing applications due to their surface chemical reactivity and excellent charge transfer properties. These materials have been explored theoretically and experimentally for gas sensing, biosensing and optical sensing (photodetectors). Two-terminal chemiresistive, three-terminal FET configuration and three-terminal electrochemical cell configurations are the popular device configurations for sensing applications. Based on sensing analytes using BOXs, these sensors can be broadly classified as gas sensors, biosensors and optical sensors. In the subsequent sections, we summarized most of the sensing applications reported on BOXs so far.

4.1 Gas Sensing

Gas sensing is an important application to assure the quality of air surrounding the atmosphere of the specimen. Gas sensors can detect specific gas molecules selectively for which it is designed. The gas-sensing phenomenon for semiconductor materials is governed either by physisorption or chemisorption activity over the material surface and response recorded in terms of change in resistance of the device. Metal oxides have been the prime choice for sensing applications due to their excellent stability and sensitivity but high-temperature operation and poor selectivity are the limitations.[72,73] Over the last two decades, 2D materials gained huge attention as a material of choice for gas sensing applications due to room temperature sensitivity and good selectivity.[74,75] Unlike other 2D materials, BOXs have not been explored to the best of their potential.

Xu et al. reported the detection of trace oxygen using 2D Bi_2O_2Se nanoplates.[69] Representation of device schematic and dynamic sensing response is given in Fig. 3a-b. The sensor shows an excellent limit of detection of 0.25 ppm for oxygen species and the detection range from 0.25 to 400 ppm. The absorption of oxygen over the Se vacancies over the surface of Bi_2O_2Se led to the change in resistance of the device. The sensing performance was tested for other gas molecules including H_2, Ar, CO_2, and CH_4 to confirm the selectivity of the devices. The sensitivity of the device was very low for other gases compared with oxygen, where the concentration of each gas was kept at 3 ppm. The sensor shows good selectivity, sensitivity, wide range of detection with excellent stability at room temperature. Further, the improved sensing response was recorded by parallel integration of sensors to improve the signal-to-noise ratio for sub-ppm detection of oxygen.

Similarly, in 2023 Bae et al. reported the morphological dependence of the CVD-grown Bi_2O_2Se nanostructures for oxygen sensing applications.[76] Among the three different morphologies (flakes, seed and bulk), vertical flakes show the highest sensing response of 0.59% and 4.93% for 10 and 100 ppm respectively with excellent detection linearity for the 10 to 100 ppm range at an operating temperature of 100° C. The vertical flakes morphology also has the advantage of fast response and recovery over the other morphologies. The higher response for flake morphology was led by the more surface area for the topmost Se^{2-} layer compared to other morphologies. The sensor shows good selectivity towards oxygen tested and compared to 50 ppm of CO_2, CH_2, H_2, and NO_2 and has negligible effect of humidity on sensing performance. The sensing reports on Bi_2O_2Se-based gas sensors show its potential to be used for the detection of trace oxygen in space, medical and semiconducting industries in the near future.

On the other hand, the first principal calculation reported for Bi_2O_2Se monolayer (ML) shows the selective detection capabilities for NO and NO_2 detection due to lower absorption energy. Sirohi et al. calculated the interaction energies for Bi_2O_2Se ML and different gas molecules to determine the selectivity.[77] Vacancy less (VL) Bi_2O_2Se ML layer shows selectivity towards NO_2 because of the lowest absorption energy of -0.48 eV. The Bi_2O_2Se ML with Se vacancies (SV) shows the lowest absorption energy of -1.59 eV for the NO gas molecule. The Se vacancies improved the selectivity and sensitivity of the Bi_2O_2Se ML. Both VL and SV Bi_2O_2Se LL show good sensitivity towards the NO gas molecules. However, BOXs are relatively new materials and less explored for gas sensing applications but the theoretical calculations show the potential of $Bi_{2-}O_2Se$ ML for the detection of toxic gases.

Recently, Wei et al. explored the humidity detection performance of flexible resistive sensors using Bi_2O_2S nanosheets.[78] The sensor shows excellent sensitivity of 2582 and fast response and recovery of 0.4 s and 2.4 s respectively for 84% RH. The sensor shows the potential for respiratory monitoring and noncontact human-machine interface applications.

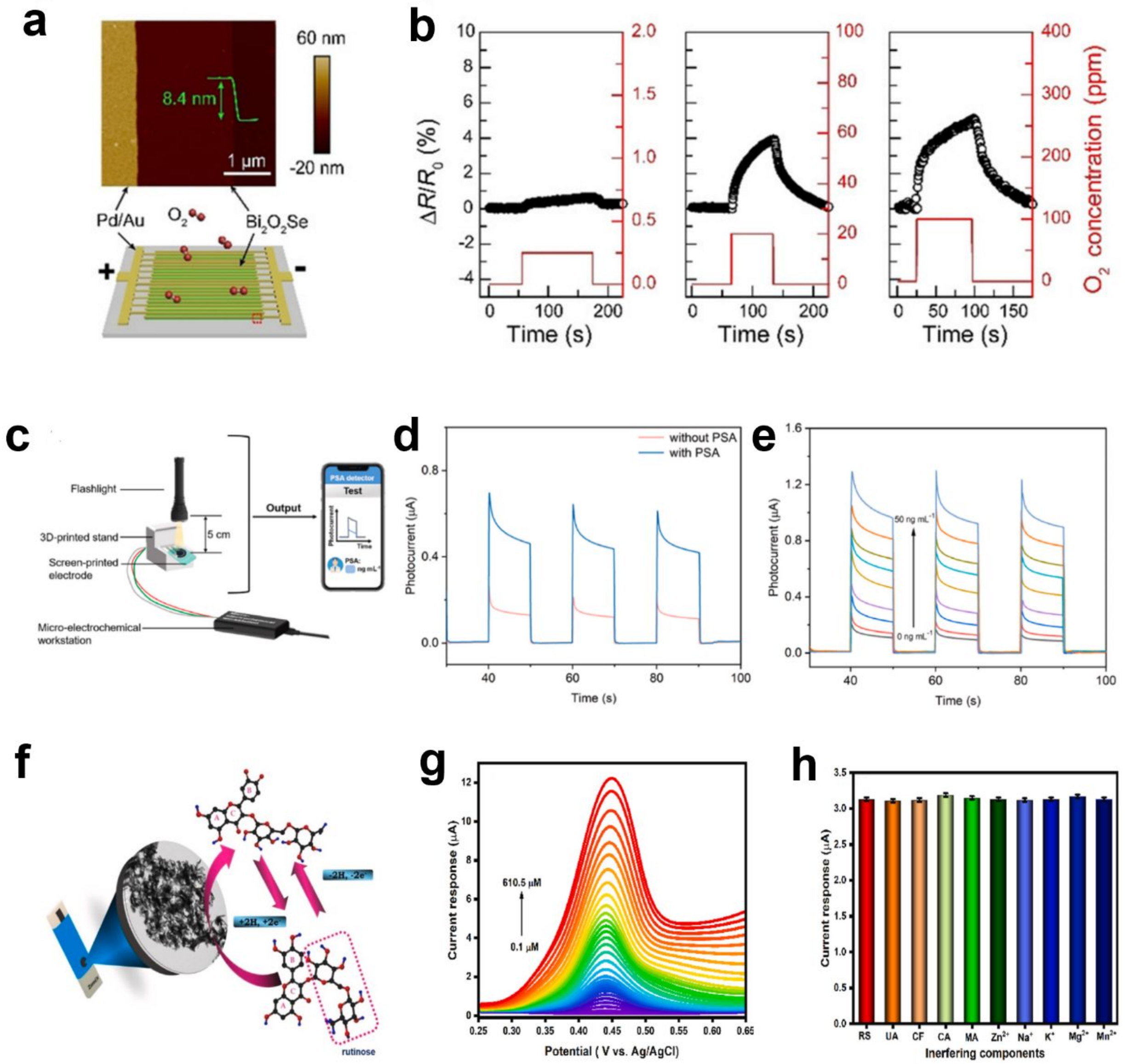

Fig. 3 (a-b) Bi_2O_2Se-based gas sensor for trace oxygen detection. Reproduced with permission.[69] Copyright 2022, Willey-VCH. (c-e) Co-doped Bi_2O_2S biosensor for PSA detection. Reproduced with permission.[70] Copyright 2023, Elsevier. (f-h) Analgesic bioflavonoid detection using Bi_2O_2S. Reproduced with permission.[71] Copyright 2023, Elsevier.

4.2 Bio-Sensing

Nanomaterials are being employed as electrode modifiers for the efficient detection of different biomarkers. In recent years, BOXs have drawn a lot of interest as an electrode modifier for the electrochemical detection of different biomarkers and analytes. Lin et al. reported the mobile-controlled portable detection of PSA using Co-doped Bi_2O_2S nanosheets as photoanode.[70] The sensing arrangement and response are shown in Fig. 3c-e. The effect of Co-doping on the structural, morphological, optical and sensing properties was reported. The Co doping led to a reduced optical bad gap from 0.90 eV to 0.86 eV upon 33% (CBOS-0.33) doping and increased photocurrent. The ascorbic acid generated through catalysis in the presence of PSA results the enhanced photocurrent. The CBOS-0.33 photoanode shows linear detection for a range of 0.2 to 50 ng mL^{-1} and a LoD of 71.2 pg ml^{-1}.

Manickaraj et al. explored the modified approach (superficial-CO_2) for the synthesis of Bi_2O_2S for the detection of Rutinoside (RS).[71] The selective detection of analgesic bioflavonoids such as Rutinoside (RS) is a great challenge. The conventional Bi_2S_3 (C-BiS) and superficial-CO_2 mediated Bi_2O_2S (SC-BiOS) were studied as electrode modifier. The observed results show the morphological and crystallite size for both samples where C–BiS has a crystallite size of 11.57 nm with the formation of nano rod-like morphology and SC-BiOS has a crystallite size of 9.03 nm with a nano-petal-like morphology. The SC-BiOS-modified electrode as shown in Fig. 3f has a higher surface area of 0.074 cm^2, lower transfer resistance and higher electron kinetics compared to C-BiS. SC-BiOS modified electrode shows an excellent detection range of 0.1-610.5 μM L^{-1} (Fig. 3g) with a detection limit of 9 and 30 nm L^{-1} with a sensitivity of 0.706 μA μM cm^{-2}. The SC-BiOS shows good selectivity (Fig. 3h), repeatability, and recovery of 98.87% and can be used for real-time application.

Similarly, Huang et al. studied the Fe-loaded Bi_2O_2S nanosheets for prostate-specific antigen (PSA) detection. PSA is a secretion by cancer cells and by certain diseases and PSA levels are high in the human serum of particular having cancer.[79] Hence, the efficient detection of PSA levels can be useful in cancer diagnosis, treatment and monitoring. The developed sensing strategy involves the synthesis of Prussian blue (PB) nanoparticles by liquid reaction method. Further, the PS nanoparticles were bound by electrostatic absorption with a signaling antibody (mAb2). The trapped PSA by trapping probe (mAb1) in a removable microplate forms a sandwich structure.

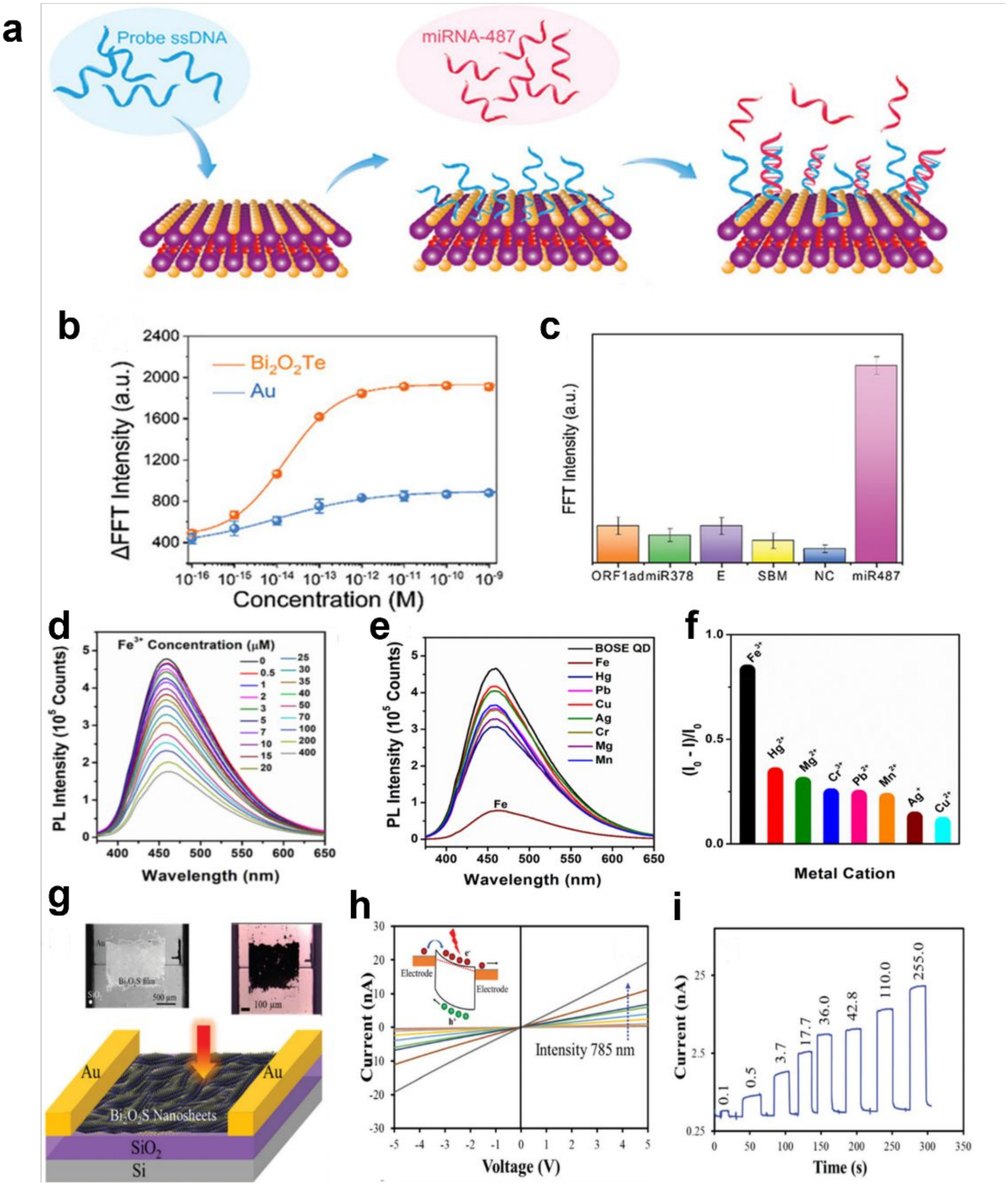

Fig. 4 (a-c) Bi_2O_2Te-based plasmonic sensor for detection of miRNA487. Reproduced with permission.[80] Copyright 2024, Willey-VCH. (d-f) Bi_2O_2Se QDs for detection of heavy metal ions. Reproduced with permission.[61] Copyright 2023, Royal Society of Chemistry. (g-i) NIR photodetection using Bi_2O_2S nanosheets. Reproduced with permission.[67] Copyright 2023, Royal Society of Chemistry.

PB nanoparticle generates oxygen radicals due to catalytic activity and oxidation of 4-chloro-1-naphthol (4-CN) to benzo-4-chloro-hexadienone (4-CD) takes place. The transfer of 4-CD to the Fe-Bi_2O_2S photoanode reduces the photocurrent as the concentration increases. The reported sensor shows a good dynamic detection range of 0.1 to 100 ng ml^{-1} with a 34.2 pg ml^{-1} limit of detection (LoD). The presented spilt incubation reaction strategy shows potential for large volume and low-cost detection of PSA. The sensor performance is comparable with the commercially available ELISA kits.

Bi_2O_2Se nanoflowers with Au nanoparticles (AuNPs) have been reported for the detection of cancer cells (MCF-7).[81] Efficient determination of circulating tumor cells (CTC) will be a significant step towards reducing casualty due to cancer and increasing cancer survival rates. Photoelectrochemical sensing approaches have been widely studied for the detection of bioassay. AuNPs/Bi_2O_2S/ITO photoanode was used as a sensing platform and the mercapto group aptamers (SH-Apt) were functionalized over the surface of the photoanode. The overexpressed protein in the cell membrane, leads to the trapping of MCF-7 cells and the level of MCF-7 cells significantly reduces the photocurrent. The sensor shows a linear detection range from 50 - 6×10^5 cell mL^{-1} with a detection limit of 17 cell mL^{-1}. The proposed sensing platform shows good sensitivity, selectivity and stability towards MCF-7 cell detection.

Wang et al. reported ultrasensitive biosensing properties of CVD-grown 2D Bi_2O_2Te for the detection of biomolecules.[80] The alteration in the ferroelectric polarization of Bi_2O_2Te upon interaction with miRNA led to a change in plasmonic response. The change in plasmonic response was recorded as a function of the concentration of miRNA487. The proposed sensor has an exceptionally lower LoD of 0.1 fM for miRNA487 and 1fM for CEA biomolecules with good selectivity. The sensing performance of the Bi_2O_2Te biosensor is shown in Fig. 4(a-c). Similarly, they explored the plasmonic detection properties of Bi_2O_2Se for the detection of bovine serum albumin (BSA).[82] The sensor has a LoD of 1 fM for BSA with a short response time.

Shi et al. demonstrated a self-powered photoelectrochemical sensor for the selective and sensitive detection of tetracycline using Bi_2O_2S/Bi_2O_3 heterostructure.[83] The sensor has a linear detection range from 0.1 pM to 200 nM and LoD of 0.5 pM. Bi_2O_2S nanosheets have been explored for the detection of Cardiac Troponin i and Carcinoembryonic antigens with a good linear detection range.[84,85]

H_2O_2 is an important biomarker for the diagnosis of different diseases and the efficient detection of H_2O_2 has significant importance for healthcare, environmental and food industries. Chitara et al. reported the nonenzymatic electrochemical detection of H_2O_2 using 2D Bi_2O_2Se nanosheets.[86] Cyclic voltammetry was employed to analyze the amount of H_2O_2 at a reduction potential of -0.68 Vs Ag/AgCl in PBS buffer (pH 7.4). The Bi_2O_2Se nanosheets modified GCE shows the linear detection for a range of 50-500 μM with the sensitivity of 100 $\mu A\ mM^{-1}\ cm^{-2}$. The selectivity of the sensor was analyzed with the other interfering analytes like NaCl, dopamine, uric acid and ascorbic acid. The sensor shows excellent selectivity towards H_2O_2. Further, the potential of this sensor for real-time application was studied by artificial sweat where the change in current was observed within the change in H_2O_2 concentrations. The H_2O_2 detection capabilities of 2D Bi_2O_2Se nanosheets show the potential to be used for the development of glucose sensors.

4.3 Optical Sensing

Optical sensing or photodetection is an important category among all sensing applications. Optical sensors are the devices used the detect the wide range of electromagnetic radiation from ultraviolet (UV) to infrared (IR).[87,88] The development of optical sensors with broadband detection capabilities is a necessity of the modern era to facilitate advanced communication technologies. Over the years, a variety of semiconductor materials have been explored for photodetection but 2D BOXs have gained huge attention in a few years for their application as photodetector. The detection range of 2D TMDCs is limited upto the NIR region but the bandgap tunability of BOXs from 2.3 eV to 0.16 eV makes it suitable for broadband detection.[89,90]

2D Bi_2O_2Se is the most popular and extensively studied for optoelectronic applications among the BOXs family.[91] Wu et al. reported the first photodetection report on Bi_2O_2Se. The device shows excellent responsivity of 2000 $A\ W^{-1}$ at 532 nm wavelength.[92] Khan et al. reported the gate tunable Bi_2O_2Se phototransistor has a maximum responsivity of 22100 $A\ W^{-1}$ and photoconductivity of 3.4×10^{15} Jones with an on/off ratio of 10^9.[56] The tuning of photocurrent using gate voltage significantly reduced the high dark current and hence high on/off ratio was achieved. The band gap of Bi_2O_2Se is suitable for the detection in the IR region, which the conventional silicon-based devices are unable to detect. Yin et al. tried for the first time to extend the detection wavelength upto 1700 nm using 2D Bi_2O_2Se.[93] They observed the responsivity of

5800 A W^{-1}, 4 A W^{-1} and 0.1 A W^{-1} for 532 nm, 1310 nm and 1550 nm wavelength respectively. Further, Chen et al. reported the IR to THz detection, where the proposed mechanism shows the generation of carrier is led by absorption for the IR region and electromagnetically induced well-injected electrons for the THz region.[55] The responsivity of the device was reported as 50 AW^{-1} at 1550 nm and 10^4 VW^{-1} at 0.17 THz.

Tian et al. reported the photodetection performance of 2D Bi_2O_2Te grown on Si substrate. The sputtered Bi_2Te_3 layer was annealed for 10 min at 400 °C in atmospheric conditions for transformation to Bi_2O_2Te.[59] The device shows good detectivity for a range from UV (210 nm) to SWIR (2400 nm). The responsivity of 3×10^5 A W^{-1} was reported for UV while 2×10^4 A W^{-1} for SWIR. Later, Yang et al. reported the self-powered photoelectrochemical photodetector based on 2D Bi_2O_2Te cells with quasi-solid electrolyte. The reported device shows responsivity of 20.5 mA W^{-1} (zero bias) and fast rise/decay times of 6/90 ms under 365 nm irradiation.[94] Apart from the pristine BOXs, various 2D/2D heterostructured configurations have also been studied for improved device performance and low dark current.[94]

Paul et al. explored the detection of heavy metal ions using Bi_2O_2Se quantum dots (QDs) as shown in Fig. 4(d-f). Bi_2O_2Se QDs of nanometric dimensions were prepared via a top-down chemical approach.[61] The Bi_2O_2Se QDs show a selective detection of Fe^{+3} ion as a function of fluorescence quenching. The DFT calculations show that the quenching takes place due to the interaction between Fe and Se ions.

Fig 4(g-i) represents the device schematic and photodetector performance of 2D Bi_2O_2S nanosheets-based broadband photodetector.[67] Hydrothermally grown 2D Bi_2O_2S flowers on FTO substrate have been reported for the detection of NIR wavelength (850 nm) with excellent responsivity of 9.48 mA W^{-1}, specific detectivity of 9.96×10^{10} Jones and fast response time of 227.7ms.[50] The fabricated device shows good environmental stability.

5. Strategies for Improved Device Performance

The sensing performance of 2D BOXs can be improved by taken care of the following strategies:

5.1 Controlled Growth

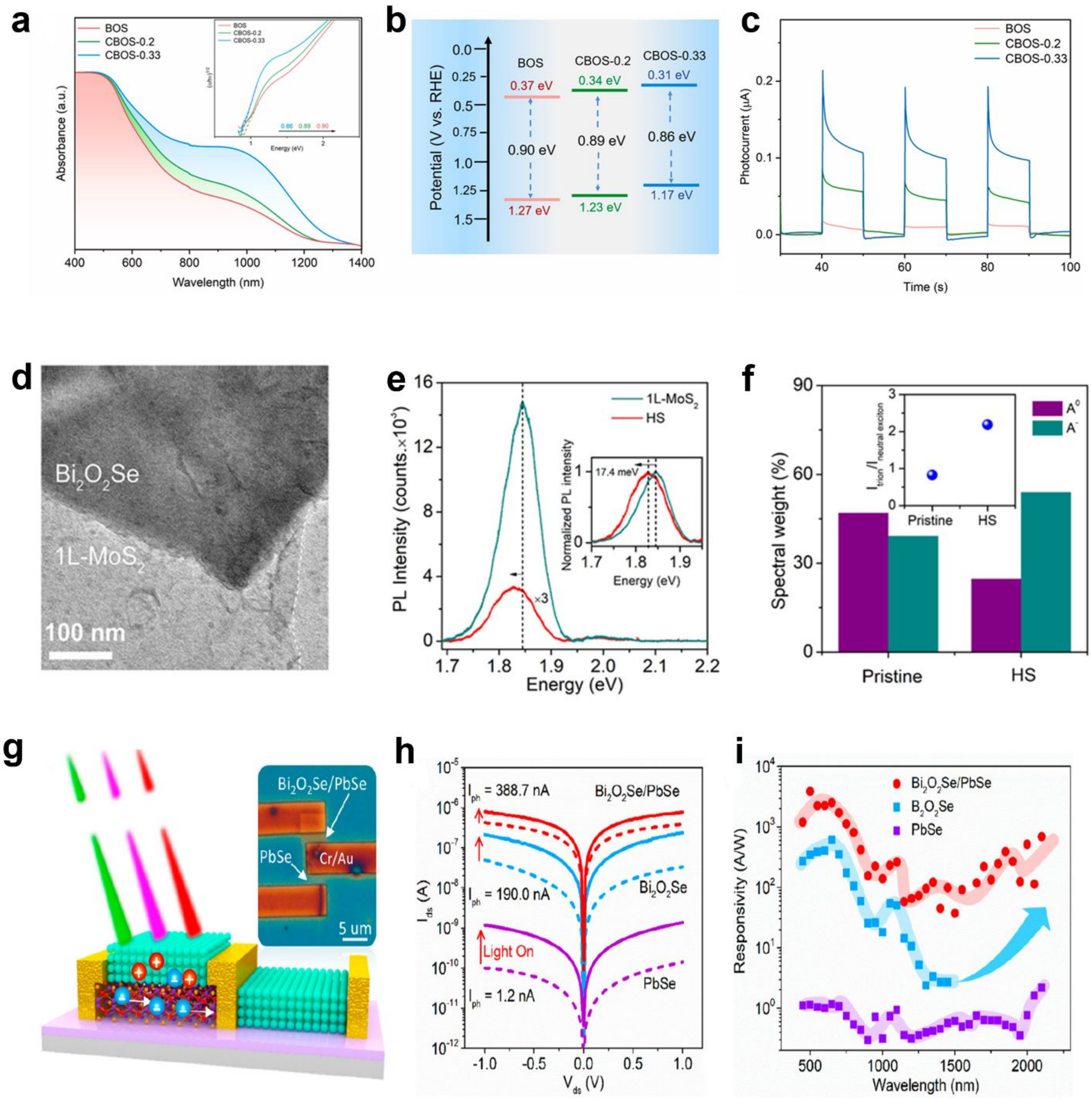

Fig.5 (a-c) Tuning of optical and electronic properties in Co-doped Bi_2O_2S nanosheets. Reproduced with permission.[70] Copyright 2023, Elsevier. (d-f) 2D/2D heterojunction using MoS_2/Bi_2O_2Se heterojunction.[95] Copyright 2023, American Chemical Society. (g-i) PbSe QDs modified Bi_2O_2Se photodetector. Reproduced with permission.[96] Copyright 2019, American Chemical Society.

The controlled growth of semiconductor materials is an important parameter for sensing applications. The sensing performance of a material depends on the active sites and hence defect density. The defects-induced modulation in electronic properties causes significant alteration in sensing properties. In the discussion of sensing applications, the Se vacancies significantly alter the sensing performance of the device. Furthermore, the surface morphologies also correlate with the sensing performance and hence the controlled growth is a must for reproducible devices with similar performance.

5.2 Doping

Doping is a well-established approach for tuning the semiconducting properties of the materials. Substitutional doping significantly alters the surface absorption energies and can help to improve the sensing performance. So far, doping in BOXs has not been explored properly. The doping strategies and their effect on fundamental properties reported recently on sensing applications show significant improvement as shown in Fig. 5(a-c). [37] There are other reports available on doping for catalytic and energy applications.[97,98]

5.3 Heterostructures or Composites

A combination of BOXs with other suitable materials can be a suitable strategy to improve the device's performance. It involves heterojunction formation, surface functionalization, decoration and mixing with other materials of different or the same dimensionality. The heterojunction formation with other 2D materials with BOXs shows an improved charge transfer as shown in Fig. 5(d-f).[95] It can further resolve the issue of large dark current in photodetection devices. CVD is one of the promising techniques for the controlled growth of BOXs heterojunctions. Wet and dry transfer, drop casting, hydrothermal and mechanical mixing also have the potential to be used to form heterostructures and composites. Decoration with lower dimensional materials can also be a significant approach to improve the sensing performance (Fig. 5(g-i)).[96]

For the real-time sensing application, a sensor needs to meet the various figures of merit including sensitivity, selectivity and operating temperature. These parameters depend on the properties of the sensing layer. The formation of heterostructures can improve the sensing performance because it has a significant effect on the various functions involved in the sensing process. 2D BOXs nanosheets have a large surface-to-volume ratio and active sites for absorption. The formation of heterostructures with other materials can tune the interaction ability and selectivity of the specific gas. The change in carrier concentration and built-in potential at the interfaces of heterostructure significantly alters the sensing ability and signal conversion performance of the sensor. Hence, the design of 2D BOXs heterostructures with receptor materials can significantly improve the sensing response. Table 1 summarises recent studies published on BOXs based sensing applications.

Table 1. Comparison of the sensing studies using BOXs.

Sensing Category	Material	Sensing Mechanism	Detection Species	Ref.
Gas Sensing	Bi_2O_2Se	Resistive Sensing	O_2	69
	Bi_2O_2Se	Resistive Sensing	O_2	76
	Bi_2O_2Se (theoretical)	Resistive Sensing	NO_2 and NO	77
	Bi_2O_2S	Resistive Sensing	Humidity	78
Bio-Sensing	Bi_2O_2Te	Plasmonic Detection	miRNA487	80
	Bi_2O_2Se	Plasmonic Detection	BSA	82
	Bi_2O_2S	Photoelectrochemical	MCF-7	81
	Fe-Bi_2O_2S	Photoelectrochemical	PSA	79
	Ag_2O -Bi_2O_2S	Photoelectrochemical	PSA	99
	Co-Bi_2O_2S	Photoelectrochemical	PSA	70
	Bi_2O_2S/ Bi_2O_3	Photoelectrochemical	Tetracycline	83
	Bi_2O_2S	Electrochemical	Bioflavonoid	71
	Bi_2O_2Se	Electrochemical	H_2O_2	86
Optical Sensing	Bi_2O_2S	Photodetector	NIR	67
	Bi_2O_2Se	Photodetector	SWIR	100
	Bi_2O_2Te	Photodetector	SWIR	101
	Bi_2O_2Se	Fluoroscence	Fe^{3+}	61

6. Conclusion and Outlook

In this mini-review, we discussed the potential of BOXs in sensing and next-generation flexible and wearable electronics. To address the recent developments reported, various synthesis and growth approaches were discussed briefly. The structural, electronic and charge properties were discussed along with the thickness dependence. BOXs have ultrahigh carrier mobility, excellent stability and band gap tunability upto 0.16 eV compared to conventional 2D materials. Due to these excellent material properties, 2D BOXs have been studied for different electronic applications, including sensing, photodetection, transistor and logic devices. Among the BOXs family, 2D Bi_2O_2Se nanosheets is the most reported and studied member of this family. It has been extensively studied for photodetection applications. As known, this is a relatively new category of semiconductor material and hence they are less explored for gas sensing and biosensing applications. In this review, we discussed the reported experimental and theoretical studies for sensing applications. Based on observation during the preparation of this article, the following avenues can be explored for the development of efficient sensing devices: 1) Theoretically BOXs-based gas sensors have low absorption energies for NO_2 and NO gas molecules and hence these can be explored for sensing device optimization. 2) The experimental report evident the significant surface and band gap tunability for these materials can be a useful strategy for the development of efficient sensing devices for environmental and health monitoring.

BOXs nanosheets can be a material of choice because of their excellent electronic properties for gas sensing, biosensing and optical detection devices. They have the potential to match the downscaling requirement and the alteration in the material by different means, i.e., doping, defects and functionalization can further help to obtain selective and highly sensitive sensors. The controlled alteration or modification can improve the surface reactivity for the target species for detection. 2D BOXs have ample scope to be used as a multifunctional material for commercial electronic devices and its full potential is yet to be explored. A joint effort from academic and industrial research can accelerate the development process to overcome the limitations for future applications.

Acknowledgements

The authors thank the financial support by the U.S. National Science Foundation (Award #2122044). This research was partially sponsored by the Army Research Office (ARO) and was accomplished under Grant W911NF2210109. The views and conclusions contained in this document are those of the authors and should not be interpreted as representing the official policies, either expressed or implied, of the ARO or the U.S. Government. The U.S. Government is authorized to reproduce and distribute reprints for Government purposes notwithstanding any copyright notation herein.

References

1 J. S. Kilby, IEEE Trans Electron Devices, 1976, **23**, 648–654.

2 International Roadmap for Devices and Systems (IRDS™) 2020 Edition - IEEE IRDS™, https://irds.ieee.org/editions/2020.

3 A. D. Franklin, Science, 2015, **349**, 6249.

4 M. Long, P. Wang, H. Fang and W. Hu, Adv Funct Mater, 2019, **29**, 1803807.

5 C. Wu, X. Zhang, R. Wang, L. J. Chen, M. Nie, Z. Zhang, X. Huang and L. Han, Nanotechnology, 2021, **33**, 072001.

6 M. R. Kumar, S. Singh, H. M. Fahmy, N. K. Jaiswal, S. Akin, A. E. Shalan, S. Lanceros-Mendez and M. Salado, J Power Sources, 2023, **556**, 232256.

7 C. C. Chiang, V. Ostwal, P. Wu, C. S. Pang, F. Zhang, Z. Chen and J. Appenzeller, Appl Phys Rev, 2021, **8**, 021306.

8 K. S. Novoselov, A. K. Geim, S. V. Morozov, D. Jiang, Y. Zhang, S. V. Dubonos, I. V. Grigorieva and A. A. Firsov, Science, 2004, **306**, 666–669.

9 L. Li, W. Han, L. Pi, P. Niu, J. Han, C. Wang, B. Su, H. Li, J. Xiong, Y. Bando and T. Zhai, InfoMat, 2019, **1**, 54–73.

10 C. Liu, H. Chen, S. Wang, Q. Liu, Y. G. Jiang, D. W. Zhang, M. Liu and P. Zhou, Nat Nanotechnol, 2020, **15**, 545–557.

11 L. Pi, L. Li, K. Liu, Q. Zhang, H. Li and T. Zhai, Adv Funct Mater, 2019, **29**, 1904932.

12 Y. Pei, X. Zhang, Z. Hui, J. Zhou, X. Huang, G. Sun and W. Huang, ACS Nano, 2021, **15**, 3996–4017.

13 Y. Li, M. Gu, X. Zhang, J. Fan, K. Lv, S. A. C. Carabineiro and F. Dong, Materials Today, 2020, **41**, 270–303.

14 M. Luo, T. Fan, Y. Zhou, H. Zhang and L. Mei, Adv Funct Mater, 2019, **29**, 1808306.

15 K. Zhang, Y. Feng, F. Wang, Z. Yang and J. Wang, J Mater Chem C, 2017, **5**, 11992–12022.

16 R. Samal, G. Sanyal, B. Chakraborty and C. S. Rout, J Mater Chem A, 2021, **9**, 2560–2591.

17 R. Prasanna, A. Gold-Parker, T. Leijtens, B. Conings, A. Babayigit, H. G. Boyen, M. F. Toney and M. D. McGehee, J Am Chem Soc, 2017, **139**, 11117–11124.

18 X. Duan, C. Wang, A. Pan, R. Yu and X. Duan, Chem Soc Rev, 2015, **44**, 8859–8876.

19 X. Cui, G. H. Lee, Y. D. Kim, G. Arefe, P. Y. Huang, C. H. Lee, D. A. Chenet, X. Zhang, L. Wang, F. Ye, F. Pizzocchero, B. S. Jessen, K. Watanabe, T. Taniguchi, D. A. Muller, T. Low, P. Kim and J. Hone, Nat Nanotechnol, 2015, **10**, 534–540.

20 D. Jariwala, V. K. Sangwan, L. J. Lauhon, T. J. Marks and M. C. Hersam, ACS Nano, 2014, **8**, 1102–1120.

21 T. Ohta, A. Bostwick, T. Seyller, K. Horn and E. Rotenberg, Science, 2006, **313**, 951–954.

22 F. Schwierz, Nature Nanotechnology 2010 5:7, 2010, **5**, 487–496.

23 S. Zhang, J. Yang, R. Xu, F. Wang, W. Li, M. Ghufran, Y. W. Zhang, Z. Yu, G. Zhang, Q. Qin and Y. Lu, ACS Nano, 2014, **8**, 9590–9596.

24 F. Xia, H. Wang and Y. Jia, Nature Communications 2014, **5**, 1–6.

25 F. Wang, S. Yang, J. Wu, X. Hu, Y. Li, H. Li, X. Liu, J. Luo and T. Zhai, InfoMat, 2021, **3**, 1251–1271.

26 M. T. Hossain, T. Jena and P. K. Giri, Small Struct, 2024, 2300511.

27 D. Verma, B. Liu, T. C. Chen, L. J. Li and C. S. Lai, Nanoscale Adv, 2022, **4**, 3832–3844.

28 J. Wu, H. Yuan, M. Meng, C. Chen, Y. Sun, Z. Chen, W. Dang, C. Tan, Y. Liu, J. Yin, Y. Zhou, S. Huang, H. Q. Xu, Y. Cui, H. Y. Hwang, Z. Liu, Y. Chen, B. Yan and H. Peng, Nat Nanotechnol, 2017, **12**, 530–534.

29 Y. Liang, Y. Chen, Y. Sun, S. Xu, J. Wu, C. Tan, X. Xu, H. Yuan, L. Yang, Y. Chen, P. Gao, J. Guo and H. Peng, Advanced Materials, 2019, **31**, 1901964.

30 C. Tan, M. Tang, J. Wu, Y. Liu, T. Li, Y. Liang, B. Deng, Z. Tan, T. Tu, Y. Zhang, C. Liu, J. H. Chen, Y. Wang and H. Peng, Nano Lett, 2019, **19**, 2148–2153.

31 Q. Wei, R. Li, C. Lin, A. Han, A. Nie, Y. Li, L. J. Li, Y. Cheng and W. Huang, ACS Nano, 2019, **13**, 13439–13444.

32 M. Wu and X. C. Zeng, Nano Lett, 2017, **17**, 6309–6314.

33 X. Yang, L. Qu, F. Gao, Y. Hu, H. Yu, Y. Wang, M. Cui, Y. Zhang, Z. Fu, Y. Huang, W. Feng, B. Li and P. Hu, ACS Appl Mater Interfaces, 2022, **14**, 7175–7183.

34 X. Zhang, Y. Liu, G. Zhang, Y. Wang, H. Zhang and F. Huang, ACS Appl Mater Interfaces, 2015, **7**, 4442–4448.

35 M. T. Hossain, T. Jena, U. Nath, M. Sarma and P. K. Giri, Nanoscale, 2023, **15**, 11222–11236.

36 M. T. Hossain, T. Jena, S. Debnath and P. K. Giri, J Mater Chem C Mater, 2023, **11**, 6670–6684.

37 M. Q. Li, L. Y. Dang, G. G. Wang, F. Li, M. Han, Z. P. Wu, G. Z. Li, Z. Liu and J. C. Han, Adv Mater Technol, 2020, **5**, 2000180.

38 W. Ai, J. Chen, X. Dong, Z. Gao, Y. He, Z. Liu, H. Fu, F. Luo and J. Wu, Nano Lett, 2022, **22**, 7659–7666.

39 L. Xu, S. Liu, H. Zhang, X. Zhang, J. Li, J. Yan, B. Shi, J. Yang, C. Yang, L. Xu, X. Sun and J. Lu, Physical Chemistry Chemical Physics, 2020, **22**, 7853–7863.

40 J. Wu, C. Tan, Z. Tan, Y. Liu, J. Yin, W. Dang, M. Wang and H. Peng, Nano Lett, 2017, **17**, 3021–3026.

41 H. Fu, J. Wu, H. Peng and B. Yan, Phys Rev B, 2018, **97**, 241203(R). DOI:10.1103/PhysRevB.97.241203.

42 T. Tong, M. Zhang, Y. Chen, Y. Li, L. Chen, J. Zhang, F. Song, X. Wang, W. Zou, Y. Xu and R. Zhang, Appl Phys Lett, 2018, **113**, 072106. DOI:10.1063/1.5042727.

43 X. Zou, F. Tian, H. Liang, Y. Li, Y. Sun and C. Wang, ACS Nano, 2022, **16**, 19543–19550.

44 T. Ghosh, M. Samanta, A. Vasdev, K. Dolui, J. Ghatak, T. Das, G. Sheet and K. Biswas, Nano Lett, 2019, **19**, 5703–5709.

45 C. Chen, M. Wang, J. Wu, H. Fu, H. Yang, Z. Tian, T. Tu, H. Peng, Y. Sun, X. Xu, J. Jiang, N. B. M Schröter, Y. Li, D. Pei, S. Liu, S. A. Ekahana, H. Yuan, J. Xue, G. Li, J. Jia, Z. Liu, B. Yan, H. Peng and Y. Chen, Sci Adv, 2018, **4**, eaat8355.

46 P. Li, A. Han, C. Zhang, X. He, J. Zhang, D. Zheng, L. Cheng, L. J. Li, G. X. Miao and X. X. Zhang, ACS Nano, 2020, **14**, 11319–11326.

47 X. Mu, C. Li, L. Wang, R. Zhang, Y. Huang, X. Yu, P. K. Wong and L. Ye, J Hazard Mater, 2022, **440**, 129808.

48 H. Xie, M. Liu, B. You, G. Luo, Y. Chen, B. Liu, Z. Jiang, P. K. Chu, J. Shao and X. F. Yu, Small, 2020, **16**, 1905208.

49 K. Zhang, C. Hu, X. Kang, S. Wang, Y. Xi and H. Liu, Mater Res Bull, 2013, **48**, 3968–3972.

50 P. Rong, S. Gao, M. Zhang, S. Ren, H. Lu, J. Jia, S. Jiao, Y. Zhang and J. Wang, J Alloys Compd, 2022, **928**, 167128.

51 W. Zhang, D. Liu, W. Jin, D. Zhang, T. Sun, E. Liu, X. Hu and H. Miao, Int J Hydrogen Energy, 2024, **51**, 1545–1557.

52 G. Zhang, N. Zhao, K. Wang and J. Li, Appl Phys A Mater Sci Process, 2023, **129**, 1–9.

53 B. Chitara, A. K. Shringi, B. Roy, M. H. Wu and F. Yan, Mater Lett, 2023, **346**, 134545.

54 P. C. Kumar, S. Senapati, D. Pradhan, J. Kumar and R. Naik, J Alloys Compd, 2023, **968**, 172166.

55 Y. Chen, W. Ma, C. Tan, M. Luo, W. Zhou, N. Yao, H. Wang, L. Zhang, T. Xu, T. Tong, Y. Zhou, Y. Xu, C. Yu, C. Shan, H. Peng, F. Yue, P. Wang, Z. Huang and W. Hu, Adv Funct Mater, 2021, **31**, 2009554.

56 U. Khan, Y. Luo, L. Tang, C. Teng, J. Liu, B. Liu and H. M. Cheng, Adv Funct Mater, 2019, **29**, 1807979.

57 J. C. Park, S. Kim, H. Choi, Y. Jung, I. Oh, J. B. Hwang and S. Lee, Cryst Growth Des, 2023, **23**, 2092–2098.

58 Y. Song, Z. Li, H. Li, S. Tang, G. Mu, L. Xu, W. Peng, D. Shen, Y. Chen, X. Xie and M. Jiang, Nanotechnology, 2020, **31**, 165704.

59 P. Tian, H. Wu, L. Tang, J. Xiang, R. Ji, S. P. Lau, K. S. Teng, W. Guo, Y. Yao and L. J. Li, J Mater Chem C, 2021, **9**, 13713–13721.

60 M. Kang, H. J. Chai, H. B. Jeong, C. Park, I. Y. Jung, E. Park, M. M. Çiçek, I. Lee, B. S. Bae, E. Durgun, J. Y. Kwak, S. Song, S. Y. Choi, H. Y. Jeong and K. Kang, ACS Nano, 2021, **15**, 8715–8723.

61 S. Paul, S. Nandi, M. Das, A. Bora, M. T. Hossain, S. Ghosh and P. K. Giri, Nanoscale, 2023, **15**, 12612–12625.

62 L. Pan, L. Zhao, X. Zhang, C. Chen, P. Yao, C. Jiang, X. Shen, Y. Lyu, C. Lu, L. D. Zhao and Y. Wang, ACS Appl Mater Interfaces, 2019, **11**, 21603–21609.

63 Z. Hui, X. Bu, Y. Wang, D. Han, J. Gong, L. Li, X. Li and S. Yan, Adv Opt Mater, 2022, **10**, 2201812.

64 A. Bora, S. Paul, M. T. Hossain and P. K. Giri, J. Phys. Chem. C, 2022, **126**, 12623–12634.

65 C. Huang and H. Yu, ACS Appl Mater Interfaces, 2020, **12**, 19643–19654.

66 A. Kumar Shringi, R. Kumar, N. F. Dennis and F. Yan, Chemosensors 2024, **12**, 17.

67 B. Chitara, T. B. Limbu, J. D. Orlando, Y. Tang and F. Yan, Nanoscale, 2020, **12**, 16285–16291.

68 M. Das, A. K. Shringi and M. Kumar, IEEE Sens J, 2022, **22**, 19183–19190.

69 S. Xu, H. Fu, Y. Tian, T. Deng, J. Cai, J. Wu, T. Tu, T. Li, C. Tan, Y. Liang, C. Zhang, Z. Liu, Z. Liu, Y. Chen, Y. Jiang, B. Yan and H. Peng, Angew. Chem. Int. Ed., 2020, **59**, 17938–17943.

70 Q. Lin, Z. Yu, L. Lu, X. Huang, Q. Wei and D. Tang, Biosens Bioelectron, 2023, **230**, 115260.

71 S. S. M. Manickaraj, S. Pandiyarajan, A. H. Liao, A. R. Panneer Selvam, S. T. Huang, J. R. Vimala, K. Y. Lee and H. C. Chuang, Chemosphere, 2023, **328**, 138534.

72 V. S. Bhati, M. Kumar and R. Banerjee, J Mater Chem C, 2021, **9**, 8776–8808.

73 A. Dey, Materials Science and Engineering: B, 2018, **229**, 206–217.

74 A. Kumar, A. Mirzaei, M. H. Lee, Z. Ghahremani, T. U. Kim, J. Y. Kim, M. Kwoka, M. Kumar, S. S. Kim and H. W. Kim, J Mater Chem A Mater, 2024, **12**, 3771–3806.

75 X. Liu, T. Ma, N. Pinna and J. Zhang, Adv Funct Mater, 2017, **27**, 1702168.

76 J. K. Bae, H. H. Cho, H. Shin, Y. Kim, H. Ko, S. J. Lee, D. D. Megersa, G. T. Gudena, S. Chae, I. S. Cho and H. K. Yu, Sens Actuators B Chem, 2023, **394**, 134398.

77 A. Sirohi and J. Singh, IEEE Trans Nanotechnol, 2022, **21**, 794–800.

78 C. Wei, M. Zhu, Z. Zhou, S. Zhao, J. Mao, D. Yin, J. Li, Y. Wang and J. Hao, Chem. Eng. J, 2021, **420**, 127655.

79 X. Huang, Q. Lin, H. Gong, L. Lu, Q. Wei and D. Tang, Anal Chim Acta, 2023, **1252**, 341058.

80 Z. Wang, L. Liu, P. Li, A. Nie, K. Zhai, J. Xiang, C. Mu, F. Wen, B. Wang, T. Xue and Z. Liu, Small, 2024, 2312175.

81 X. Xu, Z. Ding, X. Zhang, R. Zha, W. Li, L. Xu, D. Sun, X. Cai, T. Liang, Y. Wang and C. Li, Anal Chim Acta, 2023, **1251**, 340982.

82 Z. Wang, L. Liu, K. Zhai, A. Nie, J. Xiang, C. Mu, F. Wen, B. Wang, Y. Shu, T. Xue and Z. Liu, Small, 2023,**19**, 2303026.

83 B. Shi, B. Chen, X. Yan, H. Cao, H. Sun, D. Wang, C. Bi, C. Wang, Y. Wang, C. Dai and W. Liu, Mater Des, 2024, **239**, 112781.

84 Z. Yu, Q. Lin, H. Gong, M. Li and D. Tang, Biosens Bioelectron, 2023, 223, 115028.

85 L. Chi, X. Wang, H. Chen, D. Tang and F. Xue, J Mater Chem B, 2022, **10**, 10018–10026.

86 B. Chitara, T. B. Limbu, J. D. Orlando, K. Vinodgopal and F. Yan, IEEE Sens Lett, 2020, 4, 2000504.

87 J. Yao and G. Yang, Nanoscale, 2020, **12**, 454–476.

88 X. Guan, X. Yu, D. Periyanagounder, M. R. Benzigar, J. K. Huang, C. H. Lin, J. Kim, S. Singh, L. Hu, G. Liu, D. Li, J. H. He, F. Yan, Q. J. Wang and T. Wu, Adv Opt Mater, 2021, **9**, 2001708.

89 A. Parida, S. Senapati and R. Naik, Mater Today Chem, 2022, **26**, 101149.

90 F. Wang, S. Yang, J. Wu, Xiaozong Hu, Y. Li, H. Li, Xitao Liu, J. Luo and Tianyou Zhai, InfoMat, 2021, **3**, 1251–1271.

91 T. Li and H. Peng, Acc Mater Res, 2021, **2**, 842–853.

92 W. Wu, J. Yu, Y. H. Chen, Y. Liu, S. Cheng, Y. Lai, J. Sun, H. Zhou and K. He, ACS Nano, 2023, **17**, 16633–16643.

93 J. Yin, Z. Tan, H. Hong, J. Wu, H. Yuan, Y. Liu, C. Chen, C. Tan, F. Yao, T. Li, Y. Chen, Z. Liu, K. Liu and H. Peng, Nature Communications, 2018, **9**, 1–7.

94 S. Yang, S. Jiao, Y. Nie, Y. Zhao, S. Gao, D. Wang and J. Wang, Mater Horiz, 2024,**11**, 1710-1718.

95 M. T. Hossain, L. P. L. Mawlong, T. Jena, A. Bora, U. Nath, M. Sarma and P. K. Giri, ACS Appl Nano Mater, 2023, **6**, 11023–11036.

96 P. Luo, F. Zhuge, F. Wang, L. Lian, K. Liu, J. Zhang and T. Zhai, ACS Nano, 2019, **13**, 9028–9037.

97 Y. Luo, H. Han, J. Li, Q. Wang, W. Zhang and Y. Jia, Sep Purif Technol, 2023, **306**, 122734,

98 Y. Xing, X. Jiang, L. Han, X. Jin, G. Ni, Y. Peng, X. Yong and X. Wang, J Clean Prod, 2023, 400, 136631.

99 X. Huang, L. Lu, Q. Lin, Q. Wei and D. Tang, Biosens Bioelectron, 2023, **239**, 115608.

100 J. Yin, Z. Tan, H. Hong, J. Wu, H. Yuan, Y. Liu, C. Chen, C. Tan, F. Yao, T. Li, Y. Chen, Z. Liu, K. Liu and H. Peng, Nature Communications 2018, **9**, 1–7.

101 P. Tian, H. Wu, L. Tang, J. Xiang, R. Ji, S. P. Lau, K. S. Teng, W. Guo, Y. Yao and L. J. Li, J Mater Chem C, 2021, **9**, 13713–13721.